Mon. Not. R. Astron. Soc. **312**, 39–50 (2000)

Non-linear inversion for the hydrostatic structure of the solar interior

Konstantin Marchenkov,[1,2] Ian Roxburgh[1]★ and Sergei Vorontsov[1,2]
[1]*Astronomy Unit, Queen Mary, University of London, Mile End Road, London E1 4NS*
[2]*Institute of Physics of the Earth, 10 B. Gruzinskaya, Moscow 123810, Russia*

Accepted 1999 August 23. Received 1999 June 2

ABSTRACT

We present the results of a non-linear inverse analysis for the hydrostatic, spherically symmetric component of the solar internal structure using the observed p-mode frequencies. The iterative non-linear inversion technique used here is based on the succesive Born approximation description of solar p-modes developed by Roxburgh & Vorontsov. This description can give a high resolution of regions of rapid variation of seismic parameters with depth (e.g., the base of the convection zone), and accounts accurately for the strong influence of gravity perturbations on low-degree modes which penetrate deep into the solar core. The inversion procedure is non-linear; the eigenfrequency equation obtained from the Born approximation is solved by iteration. The particular target of our inverse analysis is to achieve the highest possible resolution of the region near the base of the solar convection zone, searching for possible signatures of penetrative convection, element diffusion and/or strong magnetic fields. The results of the global inversion obtained with solar p-mode frequencies provided by the recent high-quality observational data (GONG, SOI/MDI, GOLF) are presented and discussed.

Key words: Sun: interior – Sun: oscillations.

1 INTRODUCTION

Standard high-frequency asymptotic analysis is known to give a very convenient, simple and physically transparent description of solar p-modes. Even when developed to second order, the uniform asymptotic approximation remains simple enough to form the basis of an efficient non-linear inversion of the observed solar p-mode oscillation frequencies (Vorontsov 1991; Vorontsov & Shibahashi 1991; Brodsky & Vorontsov 1993; Vorontsov et al. 1994; Gough & Vorontsov 1995).

There are two principal limitations on the accuracy of these asymptotic analyses which restrict their diagnostic capability. The first is the inherent inability of any short-wavelength approximation to account for a rapid variation of the seismic papameters on a scale shorter than the wavelength. The second is related to effects of gravity perturbations, which, for modes of low degree, become too strong to be accounted for with enough accuracy. These limitations need to be overcome if an inversion for the solar structure is to extract all the information contained in the high-precision data now available in solar seismology from experiments such as GONG and those on *SOHO*.

The inversion technique which we use here is based on the more accurate description of solar p-modes developed by Roxburgh & Vorontsov (1994d, 1996, hereafter R&V96). This provides a significant improvement over the standard asymptotic analysis in that it incorporates a Born approximation to allow a detailed and accurate treatment of regions of rapid variation of seismic parameters with depth, giving an increase in resolution of the inversion near the base of the convection zone (Marchenkov et al. 1998). Higher order Born approximations give a better description of the strong influence of gravity perturbations on low-degree modes which penetrate deep into the solar core. Following the general approach developed in earlier work (Roxburgh & Vorontsov 1994a,b,c,d, 1996), the eigenfrequency equation is composite – it comes from matching the approximate solutions appropriate in solar interior with exact, non-asymptotic solutions of the adiabatic wave equations near the surface. As a result of this matching, the outer layers contribute to the eigenfrequency equation with a surface phase shift $\alpha^{\rm out}$. If, as is widely believed to be the case, all the non-adiabatic effects are localized predominantly in the surface layers, then, within this approach, they contribute only to the surface phase shift and are effectively filtered out in the inversion for the seismic stratification of the deep interior.

Section 2 outlines the description developed in (R&V96), summarizing the relations which will be used in the numerical inversion and which will be referred to in subsequent sections. The iterative inversion technique is described in Section 3. Section 4 presents the

★ E-mail: i.w.roxburgh@qmw.ac.uk

numerical results obtained with observational solar oscillation frequencies (GONG, SOI/MDI, GOLF), together with results of some artificial inversions. We summarize the results in Section 5.

2 THE EIGENFREQUENCY EQUATION

The general form of the eigenfrequency equation for p-modes of degree ℓ and radial order n is (R&V96)

$$F(\tilde{w}) \simeq \frac{\pi}{\omega}\left(n + \frac{5}{72}\frac{1}{\pi^2 n} + \alpha^{\rm int} + \alpha^{\rm out}\right), \tag{1}$$

where ω is angular frequency,

$$F(\tilde{w}) = \int_{r_1}^{R} s\,{\rm d}r, \quad s^2 = \frac{1}{c^2} - \frac{\tilde{w}^2}{r^2}, \quad \tilde{w} = \frac{\ell + 1/2}{\omega}, \tag{2}$$

c is the adiabatic sound speed, r_1 denotes the position of the lower turning point [where $s(r)$, the leading-order approximation to the radial wavenumber, vanishes], and the solar radius R is defined to be at the temperature minimum.

The surface (or outer) phase shift $\alpha^{\rm out}$ and the internal phase shift $\alpha^{\rm int}$ come from matching the approximate solutions of the adiabatic wave equations in the solar interior with the exact solutions of the wave equations in a thin layer near the solar surface, where the asymptotic analysis becomes invalid. The matching of the internal and external solutions is performed through the intermediate, leading-order asymptotic solution (with radial wavenumber s), which is locally valid with sufficient accuracy deep in the convection zone (below the He and H ionization regions).

In the eigenfrequency equation, the surface phase shift $\alpha^{\rm out}$ absorbs the difference in phase between the exact and the simplest asymptotic solutions in the near-surface layers. The theoretical modelling of the numerical values of the surface phase shift $\alpha^{\rm out}$ faces serious uncertainties related to both the solar stratification (the region of superadiabatic convection) and the physics of the oscillations in the near-surface layers (non-adiabatic effects, interaction with turbulent convection and wave leakage to the upper atmosphere). With these unknown effects in the oscillation frequencies related to the surface layers, the inversion for the internal structure using equation (1), or any other description, is made possible because for small degree ℓ the horizontal wavenumber near the surface can be neglected compared with the radial wavenumber, so the surface phase shift depends on frequency only and not on degree. This then allows the surface phase shift to be filtered out in the inversion for the interior structure, together with all the uncertainties in the stratification and in the physics of the oscillation in the outer layers (for more discussion, see Gough & Vorontsov 1995).

In the inversions described below, we will use a more detailed functional form of the surface phase shift

$$\alpha^{\rm out} = \alpha_0^{\rm out}(\omega) + \tilde{w}^2\alpha_2^{\rm out}(\omega) \tag{3}$$

which, in the leading order, incorporates its dependence on degree ℓ (Brodsky & Vorontsov 1993; Roxburgh & Vorontsov 1994a; Gough & Vorontsov 1995). With the current accuracy of the measured frequencies, such a correction is needed for all the intermediate-degree modes with turning points above the base of the convection zone. At higher degree, it gives satisfactory results until $r_1 \simeq 0.95R$. Note that the degree dependence of the surface phase shift has been neglected for simplicity in the derivation of the eigenfrequency equation (1) in R&V96; the corresponding generalization is straightforward.

The internal phase shift $\alpha^{\rm int}$ is the main new feature of the description of R&V96; this absorbs the difference in phase between the approximate solution of the wave equation in the solar interior and the simplest leading-order asymptotic solution. This internal phase shift comes from solving, using successive Born approximations, the wave equation

$$\frac{{\rm d}^2\psi}{{\rm d}z^2} + \omega^2 z\psi = U(z)\psi, \tag{4}$$

which results from the approximate reduction of the complete fourth-order system of differential equations of linear adiabatic oscillations to the second order (R&V96). In equation (4), the wave function ψ is proportional to the Eulerian pressure perturbations $p' = \rho_0(r)h_2(r)\eta(r)Y_{\ell{\rm m}}(\theta,\varphi)$, $h_2(r) = \exp\int_0^r N^2 g_0^{-1}\,{\rm d}r$, with usual notations for the unpertubed density $\rho_0(r)$, Brunt–Väisälä frequency $N(r)$ and gravitational acceleration $g_0(r)$. The wave function

$$\psi = v\eta, \quad v = \left(\frac{r^2 h z'}{\omega^2 - N^2 + 4\pi G\rho_0}\right)^{1/2}, \qquad h = \frac{h_2}{h_1}, \qquad h_1(r) = \exp\int_0^r g_0 c^{-2}\,{\rm d}r; \tag{5}$$

the independent variable in the wave equation is determined as

$$zz'^2 = s^2, \qquad z = {\rm sgn}\,(s^2)\left|\frac{3}{2}\int_{r_1}^{r}|s^2|^{1/2}\,{\rm d}r\right|^{2/3}, \tag{6}$$

and the acoustic potential $U(z)$ is

$$U(z) = \frac{1}{v}\frac{\mathrm{d}^2 v}{\mathrm{d}z^2} + \left(\frac{\mathrm{d}z}{\mathrm{d}r}\right)^{-2}\left\{\left[\frac{1}{c^2} - \frac{\ell(\ell+1)}{\omega^2 r^2}\right]N^2 - \left[\frac{1}{c^2} - \frac{\ell(\ell+1)}{\omega^2 r^2}\frac{N^2}{\omega^2}\right]4\pi G\rho_0 - \frac{1}{4r^2}\right\}. \tag{7}$$

In the simplest leading-order, high-frequency asymptotic approximation, when $U(z)$ is neglected, the wave equation (4) reduces to the Airy equation $\mathrm{d}^2\psi/\mathrm{d}z^2 + \omega^2 z\psi = 0$, with regular solution $Ai(-\omega^{2/3}z)$; the internal phase shift α^{int} is zero in this approximation. The term with 5/72 in the eigenfrequency equation (1) comes from the asymptotic behaviour of Airy functions.

The acoustic potential $U(z)$ has a finite range – it can be neglected in the region around the matching point $z = z_{\mathrm{m}}$ (taken to be somewhere in the the convection zone where a simple asymptotic solution is locally valid), which makes the results independent of z_{m}. The solutions of the wave equation (4) are determined using successive Born approximations, up to third order:

$$\psi(z) \simeq Ai(-\omega^{2/3}z) - B\cdot Bi(-\omega^{2/3}z), \qquad B = B_1 + B_2 + B_3, \quad z \approx z_{\mathrm{m}}, \tag{8}$$

$$B_1 = \pi\omega^{-2/3}\int_{-\infty}^{z_{\mathrm{m}}} Ai^2(-\omega^{2/3}z)U(z)\,\mathrm{d}z, \tag{9}$$

$$B_2 = -2\pi^2\omega^{-4/3}\int_{-\infty}^{z_{\mathrm{m}}} Ai(-\omega^{2/3}z)U(z)Bi(-\omega^{2/3}z)\int_{-\infty}^{z} Ai^2(-\omega^{2/3}z')U(z')\,\mathrm{d}z'\,\mathrm{d}z, \tag{10}$$

$$B_3 = 4\pi^3\omega^{-2}\int_{-\infty}^{z_{\mathrm{m}}} Ai(-\omega^{2/3}z)U(z)Bi(-\omega^{2/3}z)\int_{-\infty}^{z} Ai(-\omega^{2/3}z')U(z')Bi(-\omega^{2/3}z')\cdot\int_{-\infty}^{z'} Ai^2(-\omega^{2/3}z'')U(z'')\,\mathrm{d}z''\,\mathrm{d}z'\,\mathrm{d}z$$
$$+\pi^3\omega^{-2}\int_{-\infty}^{z_{\mathrm{m}}} Bi^2(-\omega^{2/3}z)U(z)\left[\int_{-\infty}^{z} Ai^2(-\omega^{2/3}z')U(z')\,\mathrm{d}z'\right]^2\mathrm{d}z. \tag{11}$$

The first-order Born approximation is given by $B = B_1$, and the second-order by $B = B_1 + B_2$.

In the vicinity of the matching point, the Airy functions $Ai(-\omega^{2/3}z)$ and $Bi(-\omega^{2/3}z)$ are replaced by their asymptotic expansions at large argument, which gives:

$$\psi \simeq z^{-1/4}\left[1 - \frac{5}{48}\frac{z^{-3/2}}{\omega}B + O\left(\frac{1}{\omega^2}\right)\right]\sin\left(\omega\int_{r_1}^{r} s\,\mathrm{d}r + \frac{\pi}{4}\right) - z^{-1/4}\left[B + \frac{5}{48}\frac{z^{-3/2}}{\omega} + O\left(\frac{1}{\omega^2}\right)\right]\cos\left(\omega\int_{r_1}^{r} s\,\mathrm{d}r + \frac{\pi}{4}\right). \tag{12}$$

Matching the internal and outer solutions leads to the eigenfrequency equation (1) with

$$\alpha^{\mathrm{int}} = \arctan\ B. \tag{13}$$

The improved accuracy of the Born approximation procedure compared with the standard second-order asymptotic analysis comes from the replacement of the second-order asymptotic term by the more accurate Born internal phase shift. The standard second-order asymptotic description is

$$F(\tilde{w}) + \frac{1}{\omega^2}\Phi(\tilde{w}) \simeq \frac{\pi}{\omega}\left(n + \frac{5}{72}\frac{1}{\pi^2 n} + \alpha^{\mathrm{out}}\right), \tag{14}$$

where $\Phi(\tilde{w})$ denotes the second-order asymptotic terms. Second-order asymptotics is a limiting case of the first-order Born approximation with the square of the Airy function squared replaced by its average.

3 THE INVERSION TECHNIQUE

The inversion procedure consists in the following steps.

(1) Determination of the surface phase shift α^{out}.
(2) Initial approximation for the function $F(\tilde{w})$ and for the sound-speed profile $c(r)$.
(3) Calculation of the internal phase shift α^{int}.
(4) Improved approximation for $F(\tilde{w})$ and for $c(r)$.

Steps 3 and 4 are then repeated until the iteration converges.

3.1 Separation of the surface phase shift

The determination of α^{out}, represented by two functions of frequency (equation 3), follows the procedure described by Gough & Vorontsov (1995) and uses the second-order asymptotic eigenfrequency equation (14). The approximation intervals were limited by $1 \le \omega/(2\pi) \le 4.5$ mHz (25–30 vector cubic B-splines), and $3000 \le \tilde{w} \le 8000$ s (10–15 splines). The optimal number of splines varies slightly between different data sets (depending on number of modes available in the approximation domain, random errors, and frequency coverage). Note that the $\tilde{w}$-range corresponds to solar p-modes with inner turning points between $r_1 \simeq 0.785R$ and $r_1 \simeq 0.955R$, where the asymptotic

description is nearly adequate even in the first order. The second-order term with functional form $\Phi(\tilde{w})/\omega^2$ allows us to extend somewhat the approximation domain in $\tilde{w}$ by using more modes with deeper turning points. When the turning point is not far enough above the base of the convection zone, the frequency is affected significantly by the rapid variation of seismic parameters there – the oscillation amplitudes are exponentially small but differ from zero. The function $\Phi(\tilde{w})$ was forced to have a smooth transition to zero values at $\tilde{w} > 4000\,\mathrm{sec}$ ($r_1 > 0.85R$), in the way described by Gough & Vorontsov.

3.2 Initial approximation

The initial approximation for the seismic stratification of the solar interior comes from the function $F(\tilde{w})$ estimated from equation (1) with the internal phase shift α^{int} set to zero. After the surface phase shift has been determined, a much wider, complete data set is used to infer $F(\tilde{w})$ in all the possible range of $\tilde{w}$; the upper limit being determined by the observational data available.

Note that for sound-speed inversions using an Abel integral transform the asymptotic function $F(\tilde{w})$ (actually, $\mathrm{d}F/\mathrm{d}\tilde{w}$) needs to be known up to its surface value at $\tilde{w}_s = R/c(R)$. At high degree $\mathcal{L}$, our theoretical description loses its accuracy; the observational data sets which we use are also limited by degree $\mathcal{L} \leq 250$. Therefore, starting with $\tilde{w} = 8500\,\mathrm{s}$ ($r_1 \simeq 0.95R$) and higher, the derivative $\mathrm{d}F/\mathrm{d}\tilde{w}$ was taken to be that computed directly from the sound-speed profile of a reference solar model. The uncertainty in the inverted sound speed which results from this matching procedure decreases with increasing depth (see Gough 1986 and Vorontsov & Zharkov 1989 for quantitative discussions); the magnitude of the uncertainty is small, because the sound speed in the convection zone is largely determined by surface gravity. This procedure specifies the outer boundary conditions for our inversion.

The frequency range of the input data is limited by the stable separation of the surface phase shift for the particular data set. Simple weights, proportional to the relative accuracy of the frequency measurements, were used in the approximation. The approximation was constrained by inner boundary conditions $\mathrm{d}F/\mathrm{d}\tilde{w} = -\pi/2$ and $\mathrm{d}^3F/\mathrm{d}\tilde{w}^3 = 0$ at $\tilde{w} = 0$ (Vorontsov 1991).

3.3 Internal phase shift

In this step we use the inverted sound-speed profile to calculate the internal acoustic potential and corresponding phase shift for each mode used in the inversion.

The overall algorithm of our seismic inversion is such that we are looking for the solution in terms of one function of radius only (the sound-speed profile). Two functions of radius are needed for the unique description of the seismic parameters of the solar interior, when adiabatic oscillation equations are appropriate. We choose the adiabatic exponent $\Gamma_1 = \Gamma_1(r)$ as a second variable. A particular profile of the adiabatic exponent $\Gamma_1(r)$ will be used as an input parameter of the inversion. We make no attempt to invert simultaneously two functions of radius. Instead, the results obtained with different input profiles of Γ_1 will be used to address the question of the diagnostic capability of the observational data in measuring the adiabatic exponent. Inversions were performed with $\Gamma_1 = 5/3$ and with $\Gamma_1(r)$ taken from a particular solar model.

From the two functions $c^2(r)$ and $\Gamma_1(r)$, the equilibrium density profile $\rho_0(r)$ can be determined by solving the equation of hydrostatic support. The Brunt–Väisälä frequency $N^2(r)$ is then determined using the relation

$$\frac{\mathrm{d}c^2}{\mathrm{d}r} = (1 - \Gamma_1)g_0 + c^2\left(\frac{1}{\Gamma_1}\frac{\mathrm{d}\Gamma_1}{\mathrm{d}r} + \frac{N^2}{g_0}\right) \tag{15}$$

(e.g. Vorontsov & Zharkov 1989). The profile of the acoustic potential $U(z)$ is then calculated using equations (5)–(7), and the phase shift α^{int} is determined using (8)–(11) and (13).

Such a complete calculation of the internal phase shift was undertaken for a few inversions to test the general convergence of the iterative scheme (see Section 4). In all other inversions, an additional simplification was used, which speeds up the numerical computations very significantly by eliminating the procedure of solving the non-linear integro-differential equation of hydrostatic support for the equilibrium density $\rho_0(r)$, which itself requires iterations. This simplification consists in taking $\rho_0(r)$, as it enters the determination of the acoustic potential through equilibrium gravitational acceleration $g_0(r)$ in equations (5) and (15) and the terms with $4\pi G\rho_0$ in equations (5) and (7), which describe the effects of gravity perturbations, directly from a reference solar model.

This simplification is based on the general property of high-frequency acoustic oscillations (trapped acoustic waves) being determined principally by the sound speed. All the effects in the wave propagation which disturb this simple property are small perturbations, described by the acoustic potential $U(z)$. On the other hand, recent solar models are known to be in a very close agreement with seismic data, with inconsistency in the sound-speed and density profiles at a level of 10^{-2} or smaller. In the inversion for the sound speed, therefore, the effect of the small inconsistency in $\rho_0(r)$ and corresponding error in the potential is negligibly small, being a product of two small quantities.

Small inaccuracies in the inverted sound speed near the upper end of the approximation domain [$r = 0.95R$, where the inverted function $F(\tilde{w})$ is matched with that predicted by a solar model] can lead, after differentiation, to significant inaccuracies in the determination of the acoustic potential in this region. Since the inverted sound speed here is only weakly constrained by the input data, this effect can finally result in a boundary-type instability in the iterative inversion. To suppress this instability, and to ensure the smooth matching of the internal solutions with leading-order asymptotic solutions deep in the convection zone, a smooth window function was applied to the computed profile of the acoustic potential. The potential $U(z)$, considered as a function of $r = r(z)$, was multiplied by the

window function taken to be 0 at $r = 0.95R$ and above, 1 at $r = 0.75R$ and below, with a (up to second derivative) smooth transition in the interval between these two points. The same window function (with an argument $r = r_1$) was imposed on the resulted internal phase shift.

For solar p-modes of degree $\ell \simeq 3$ and smaller, the effects of gravity perturbations become very strong (up to about 50 μHz in the frequencies); the accuracy provided by the Born approximation becomes insufficient even when going to the third order (R&V96). At degree $\ell \leq 10$, therefore, the more accurate computations of the internal phase shift were also performed by integrating the second-order equation (4) directly, and then matching the numerical solutions with the asymptotic behaviour of the wave functions (equation 12). Since the second-order equation (4) itself originates from an approximate (high-frequency) description of gravity perturbations, the computations were also performed by solving directly the complete fourth-order system of differential equations (R&V96). The results obtained with different approximations are compared in Section 4.

3.4 Improved approximation for the sound speed

The improved approximation for $F(\tilde{w})$ and $c(r)$ is obtained using equation (1) with the internal phase shift calculated as described above. The resulting sound-speed profile is then used to recalculate the internal phase shift. These two steps are repeated until there is no change in the sound-speed profile between successive iterations.

Particular care is needed in the spline approximation of $F(\tilde{w})$ with careful choice of the total number of B-splines and the distribution of their breakpoints. These parameters determine the regularization properties of the inversion, and control the trade-off between convergence, the stability of the inversion to random errors in the input data, and the resolving capability of the solutions. About 40 cubic B-splines were found to be appropriate, with the exact number varying slightly between different data sets: the optimal choice was selected using the requirements of the convergence of the iterative procedure and the stability of the results to random noise added to the input frequencies. To achieve the best possible resolution without losing convergence, it was found appropriate first to perform a few iterations with a smaller number of B-splines and with an additional smoothing of the resulting sound-speed profile. The same effect can be obtained by using splines with tension, which is then relaxed in the final iterations.

4 NUMERICAL RESULTS

With a proper control of the regularization properties of the inversion (selected in a few trial runs), the iterative procedure was found to converge very rapidly, in 7–8 iterations.

Several artificial inversions were performed to test the general convergence properties of the iterative technique, using as artificial data the frequencies from a standard solar model (GONG reference Model S, Christensen-Dalsgaard et al. 1996). An initial density profile $\rho_0(r)$ was taken from from a simple two-zone polytropic model with solar mass and radius, and the value of $c_1^2(r)$ was calculated using the inversion algorithm with the given frequencies. This value of $c_1^2(r)$ was then used to construct a new model in hydrostatic equilibrium and hence a new density profile $\rho_1(r)$. This new density profile was then used in the inversion algorithm to yield a new value $c_2^2(r)$. This process converged to the density and sound-speed profile of the standard model after only three iterations. The results are illustrated in Fig. 1.

To test whether the accuracy of our approximation is adequate for describing the oscillation frequencies, we compare the approximation residuals with observational errors.

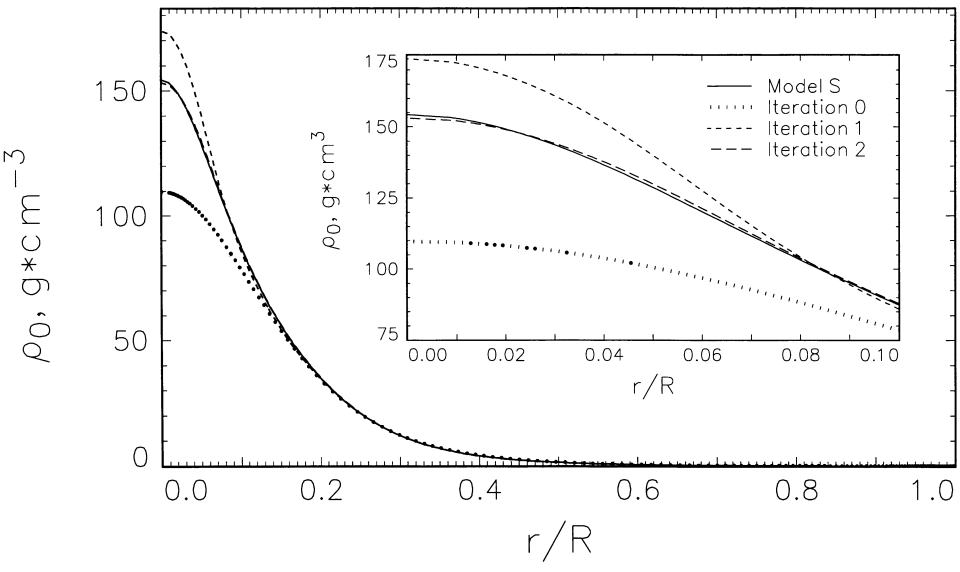

Figure 1. Convergence of density profiles used in the inversion. The dotted line shows the initial density profile, and the solid line shows the density profile of the reference solar model used in the computations of the artificial frequencies.

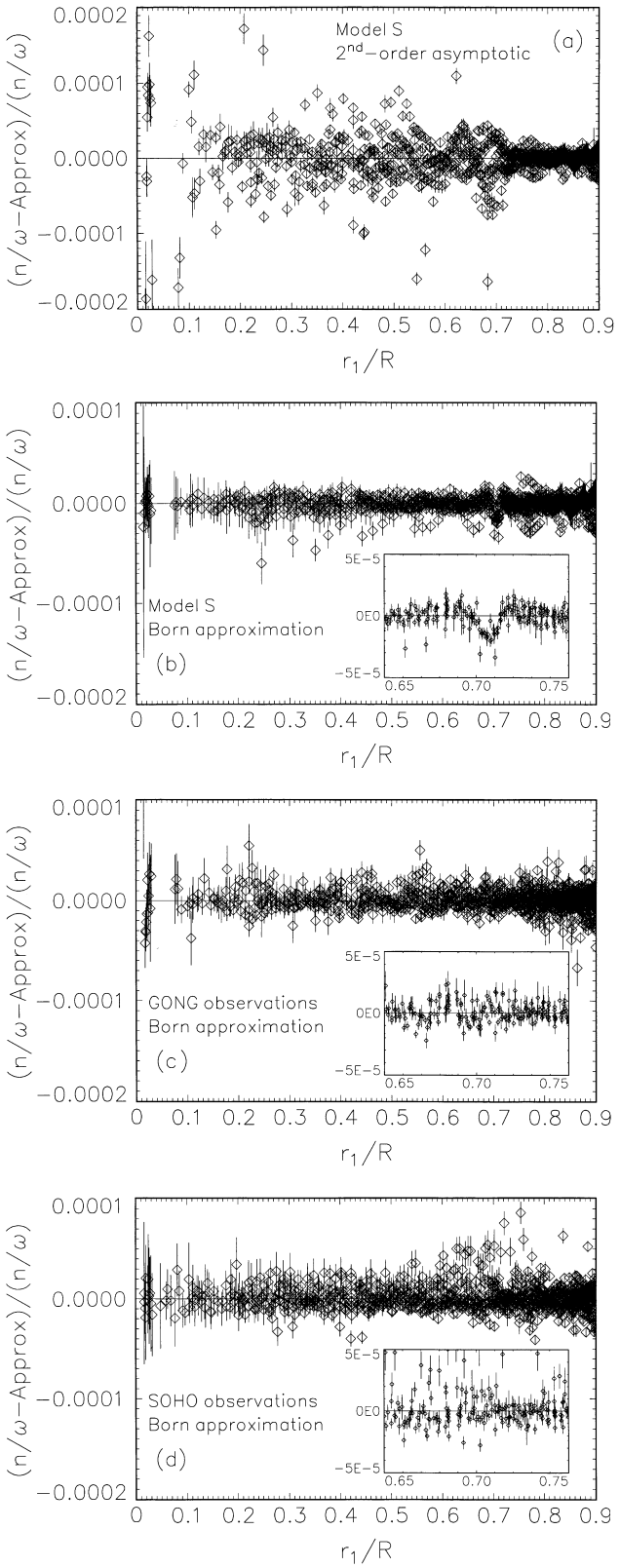

Figure 2. The final approximation residuals resulting from the iterative inversion, plotted versus the position of the lower turning point r_1. (a) Artificial inversion using second-order asymptotic description; (b) artificial inversion with the Born approximation; (c) inversion of the GONG observational data set, using the Born approximation; (d) same as (c), but with the SOI/MDI observational data set.

Fig. 2(a) shows the approximation residuals of the input data (n/ω; see equations 1 and 14) when the second-order asymptotic eigenfrequency equation (14) was used in the artificial inversion using eigenfrequencies of the reference solar model (Model S, Christensen-Dalsgaard et al. 1996). The artificial data set was limited to p-modes available in the GONG observational data set. Error bars indicate the reported observational errors. Regular structures of magnitudes much larger than the observational errors are clearly seen in the residuals for modes with turning points near and below the base of the solar convection zone.

Fig. 2(b) shows the result of the Born approximation applied to the same data set. The residuals are reduced to the level close to the observational errors. Some regular structures remain, however, in the residuals in the region around the base of the convection zone. The sharp transition in the slope of the sound-speed gradient here cannot be perfectly reproduced by the inversion, because of the wave-like nature of the input data; the sharp transition is smoothed out somewhat by the regularization property of spline approximation. Note that the parameters of the spline approximation used here were exactly the same as those chosen for the observational data (Fig. 2c): allowing better resolution in the artificial inversion would make the approximation residuals much smaller.

Fig. 2(c) shows the approximation residuals of the GONG observational data. The data set consists of 1803 modes with frequencies in the range from 1.5 to 4.0 mHz. The frequency range is limited by the stable separation of the surface phase shift, determined by the quality of the observational data available. We conclude that most of the useful information contained in the GONG observational data set has been extracted by the Born approximation. The absence of the prominent regular feature in the residuals near the base of the convection zone (compare with Fig. 2b) might indicate that the convective boundary in the real Sun as seen by the acoustic waves is not as 'sharp' as in the model.

Fig. 2(d) shows the approximation residuals of the inversion of SOI/MDI data (144 days data set, 1802 modes in the frequency range from 1.5 to 4.0 mHz), with error bars corresponding to observational errors. As with GONG data, we consider the quality of the approximation to be nearly adequate. Approximation of both observational data sets with the second-order asymptotic equation (14) leads to residuals similar to those of the artificial inversion shown in Fig. 2(a).

We now test the accuracy of the Born approximation more carefully. In Fig. 3(a) we compare the results for the sound-speed difference between the inverted and the exact values for the reference model using all the p-modes in frequency range 1.5–4.0 mHz. The results were obtained in the third Born approximation in all the degree range, with direct numerical integration of the second-order wave equation (4) for degree $\ell \leq 10$, and with direct numerical integration of the complete fourth-order system of differential equations (for $\ell \leq 10$). The significant improvement in the inverted sound speed which can be achieved in the deep interior is clearly seen. Athough the direct solution of the complete system of differential equations is more computationally expensive compared with Born approximation procedure, it has been used for $\ell \leq 10$ in all the subsequent inversions.

Fig. 3(b) illustrates the intrinsic accuracy of the artificial sound-speed inversion for different sets of eigenmodes of the reference model

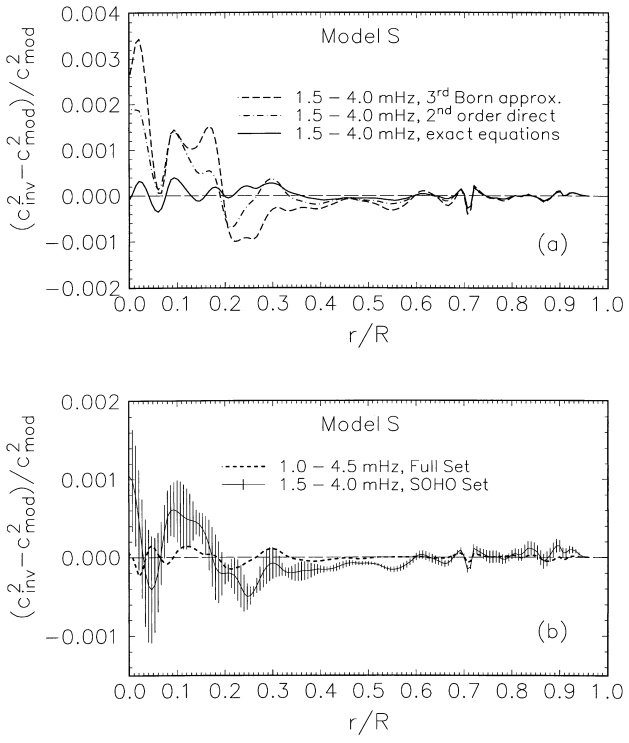

Figure 3. The accuracy of the sound-speed profile reproduced by the artificial inversion of the exact eigenfrequencies of the reference model. (a) Results obtained with using the Born approximation in all the degree range, and with using the direct numerical integration of the wave equations for $\ell \leq 10$; (b) results obtained with using p-modes available in the SOI/MDI data set, and with all the p-modes of a wider frequency range. Vertical bars indicate the stability of the inversion to random errors in the input data (see text).

used as an input data. The importance of the additional information contained in lower and higher frequencies for resolving the structure of the regions around the base of the convection zone and in the deep interior is clearly seen. In the solar core, the accuracy of the sound-speed inversion using all the p-modes in the frequency interval 1.0–4.5 mHz is about 5 times better than that obtained with p-modes which correspond to the *SOHO* observational data set (SOI/MDI combined with GOLF, frequency range 1.5–4.0 mHz). The vertical bars indicate the envelope of the solutions obtained when random errors were added to the frequencies, with the errors being given by 100 random realizations of white noise with amplitudes equal to the reported observational errors.

In the inversions of observational data, we use the solar p-mode frequencies inferred from 10 months of GONG observations (Hill et al. 1996), and a combined observational data set of *SOHO*/MDI (144 days; Rhodes et al. 1998) and low ℓ *SOHO*/GOLF frequencies (110 modes; Lazarek et al 1998), refered to as the *SOHO* data set. Fig. 4 shows the results of the sound-speed inversion obtained with the two data sets. Vertical bars mark the combined *SOHO* data set and show the envelope of the solutions obtained with white noise (as in Fig. 3b). Some difference between the results obtained with GONG and *SOHO* data is seen deep in the solar interior. Note that the 'error bars' indicate only the stability of the regularized solution to random errors, not the exact band of all the possible solutions. More data of better accuracy is needed to resolve the structure of the solar core in greater detail.

We now describe the results of our seismic inversions expressed in terms of the sound-speed gradient; this is obviously more difficult to infer accurately from the input data compared with the absolute values of the sound speed, but appears to be very convenient for discussing the possible interpretation of the results. Inversions of the solar p-mode frequencies will be represented by the results obtained with the *SOHO* data set.

In Fig. 5 we compare the the sound-speed gradient represented by the function $\tilde{W}(r) = r^2/GM \times \mathrm{d}c^2/\mathrm{d}r$ (Däppen & Gough 1984), inverted from the observational and from the artificial frequencies, with the exact profile in the reference model. We include similar results obtained with second-order asymptotic inversion used in previous studies (Vorontsov et al. 1994); the significant improvement provided by Born approximation is clearly seen.

The convenience of the traditional representation of the region around the base of the convection zone in terms of $\tilde{W}(r)$ came from the property that the convection zone contains not more than 2 per cent of the solar mass, so that the gravitational acceleration $g_0(r) \simeq GM/r^2$. With higher accuracy observational data, and taking into account the fact that the mass profile $M(r)$ is also constrained with a good accuracy by the seismic data, we find it appropriate to introduce a slightly different variable, which we designate as $W(r)$:

$$W(r) \equiv \frac{1}{g_0(r)}\frac{\mathrm{d}c^2}{\mathrm{d}r} + \frac{2}{3} = \left(\frac{5}{3} - \Gamma_1\right) + \frac{c^2}{g_0}\frac{\mathrm{d}\ln\Gamma_1}{\mathrm{d}r} + \frac{c^2}{g_0}\frac{N^2}{g_0}. \tag{16}$$

The function $W(r)$ is close to zero in the adiabatic part of the convection zone and has an abrupt variation in slope at the boundary with radiative interior (as does $\tilde{W}$). An additional advantage of the new variable is that it is also convenient for representing the solution in the deeper interior, all the way down to the solar centre. When calculating $W(r)$ from $\mathrm{d}c^2/\mathrm{d}r$, we will use $g_0(r) = GM_r/r^2$ from the reference model – an approximation which is good enough for representing the results (see discussion in Section 3.3). The inverted profiles of $W(r)$ are shown in Fig. 6.

Fig. 6a illustrates the general behaviour of $W(r)$ in the solar interior; it is determined predominantly by the Brunt–Väisälä frequency $N(r)$, since the deviations of the adiabatic exponent Γ_1 from 5/3 are rather small. Different curves which represent the results of different inversions are almost indistinguishable on this scale. The regions where we observe some significant deviations from the prediction of the reference model are indicated by three rectangles, and shown on an enlarged scale in 6(b)–(d).

Fig. 6b shows the region above the convective boundary. Note that the vertical scale is magnified here by a factor of 100, so that the effects which we will discuss are rather small. The inaccuracy of the artificial inversions is clearly seen on this scale. When the input eigenfrequencies are limited by the p-modes available in the observational (*SOHO*) data set, the position of the base of the convection zone is clearly reproduced as a sharp variation in the inverted sound-speed gradient (line marked with triple dots), but shifted in depth compared with its actual position by almost $0.01R$. Numerical experiments with different data sets show that this systematic error is due, in part, to

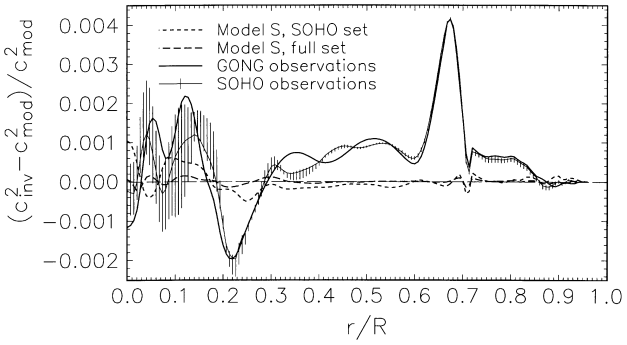

Figure 4. Results of the sound-speed inversion obtained with the observational solar p-mode frequencies, represented by the relative deviation of the inverted $c^2(r)$ from the prediction of the reference solar model. The results of the corresponding artificial inversions are shown by dashed lines to indicate the intrinsic accuracy of the inversion.

insufficient p-modes with turning points in the immediate vicinity of the sharp boundary. The accuracy is improved when all the p-modes in frequency range 1.0–4.5 mHz are used in the inversion (line marked with large dots), but the fit is still not perfect. In fact, we should not expect to reproduce exactly the reference model, since this model has a discontinuity in $W(r)$ at the base of the convective zone, due to the discontinuity in the molecular weight gradient $\mathrm{d}\mu/\mathrm{d}r$ coming from the inclusion of diffusion of *He* in the region below the zone.

Inversions of the *SOHO* observational data set are shown by the solid line with error bars [obtained with $\Gamma_1(r)$ taken from the reference model] and by the dashed line (obtained with $\Gamma_1 = 5/3$). Note that the results of these two inversions are very nearly the same (within the error bars obtained by adding random noise to the input data). The small sensitivity of the inverted sound speed to the variation of $\Gamma_1(r)$, which is used as an input parameter of the inversion, reflects the general property that the p-mode frequencies are principally determined by the sound speed alone (see also the discussion in Section 3); in the inversion a small variation of $\Gamma_1(r)$ leads to a small variation of the acoustic potential, but the potential itself is a small perturbation (in the convection zone, negligibly small). This near-stationary property of the inverted $c^2(r)$ does not prevent, however, using the inferred $c^2(r)$ for testing the adiabatic exponent implicitly, as discussed below.

The sound-speed gradient derived from the observational data deviates significantly from the prediction of the reference model below $r \simeq 0.77R$. Equation (16) shows that this discrepancy is related either to an inadequate description of the last term with $N^2(r)$, or to $\Gamma_1(r)$ (two terms). The term with $N^2(r)$ is proportional to the dimensionless value of the subadiabatic temperature gradient. If the discrepancy were due to errors in $N^2(r)$, this would imply a dimensionless superadiabatic gradient of the order of 10^{-3}, whereas the estimate from convective modelling is of order 10^{-8}. It is difficult to imagine how the superadiabatic gradient could be so large. The alternative explanation with $\Gamma_1(r)$ points to an inaccuracy coming from the equation of state. The adiabatic exponent enters the expression (16) for $W(r)$ in two terms – one with its absolute value, and another with its gradient. The separate contribution of these two terms in the reference model is shown in Fig. 6(b) by the dotted and long-dashed lines. The first term clearly dominates in the model, which indicates that it is the major factor in the discrepancy. The net result of these considerations is that in the deeper part of the convection zone the adiabatic exponent is significantly closer to 5/3 than that obtained in the model. Higher values of the adiabatic exponent in the real Sun lead to the higher absolute values of the sound speed seen in Fig. 4 below $r \simeq 0.8R$. This conclusion is in agreement with the results of the direct calibration of solar envelope models (Baturin & Vorontsov 1998) which show similar small inaccuracies in the sound speed deep in the convection zone which remain in the models computed with recent OPAL (Iglesias & Rogers 1991) equation of state.

Fig. 6(c) includes the region below the base of the convection zone. The abrupt change in slope of the sound-speed gradient is smoothed significantly by the artificial inversion; below the convective boundary, the accuracy of the inverted $W(r)$ recovers ($r < 0.7R$). Inversions of the observational frequencies performed with different input profiles of Γ_1 fall on a single curve in the scale of this figure. The inversion is very stable: error bars are also not seen on this scale. The significant difference between the inversion and the model prediction changes sign at $r \simeq 0.67R$ (at this point, the difference in the sound speed itself has its maximum value; see Fig. 4). This inconsistency can not be explained by inaccuracies in the adiabatic exponent, since these effects are expected to be at least an order of magnitude smaller (the model prediction for Γ_1 differs from 5/3 by no more than 2×10^{-3} below the H and He ionization region).The most probable explanation is an inaccuracy in hydrostatic density profile related to temperature gradient and/or chemical composition gradient.

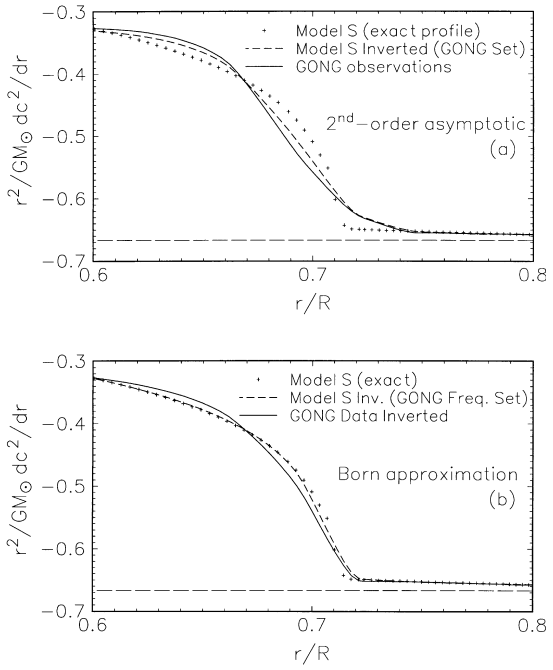

Figure 5. The sound-speed gradient described by function $\tilde{W}(r)$, inverted from the GONG p-mode frequencies (solid curve) and from the theoretical eigenfrequencies of the reference solar model (dashed curve). Crosses show the exact profile in the reference model. (a) Second-order asymptotic analysis; (b) Born approximation.

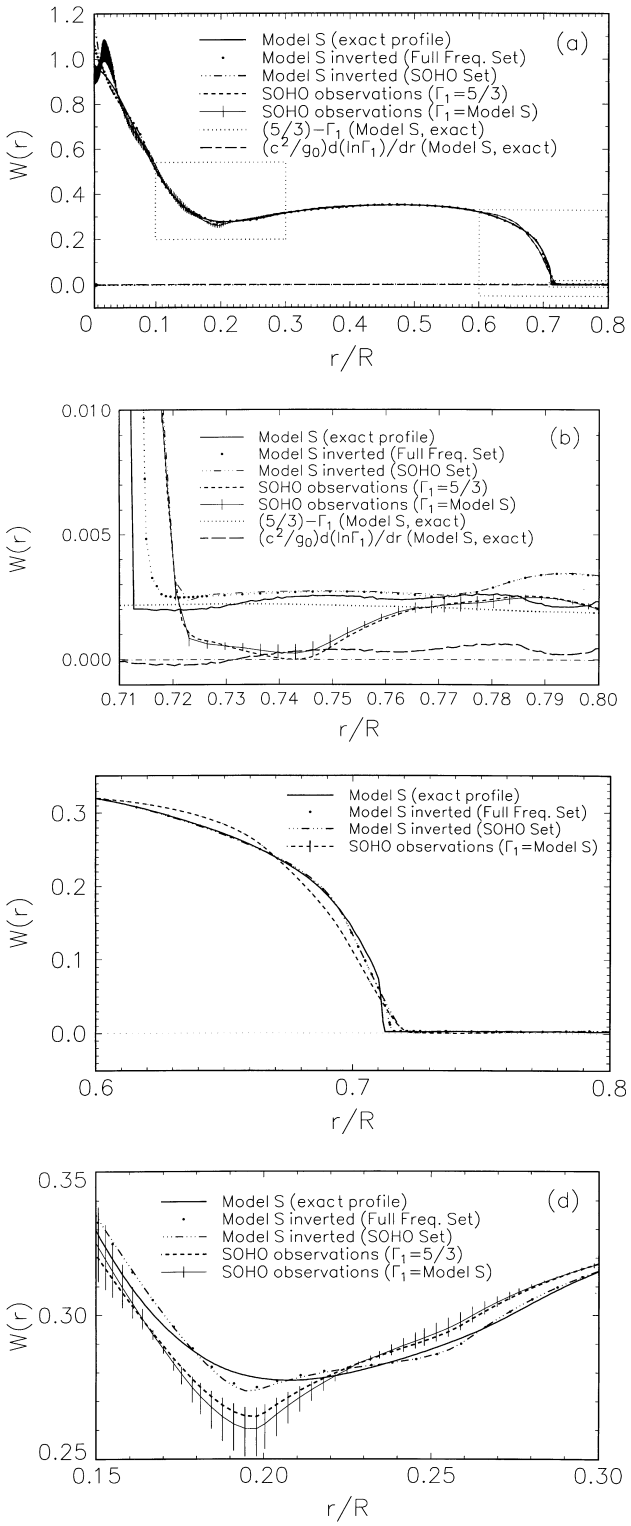

Figure 6. The sound-speed gradient described by function $W(r)$. Rectangles (a) indicate three regions shown on a better scale in (b)–(d). Different curves represent the reference model, results of the artificial inversions, and the solar profile inverted from the *SOHO* observational data set (see text).

The prominent inaccuracy of the $c^2(r)$ predicted by the reference model (0.4 per cent at $r \simeq 0.67R$) is in complete agreement with previous findings, which were based on linearized sound-speed inversions; different explanations have been considered, related to inadequate gradient of He abundance in the model, effects of mass loss, or just opacity errors (Gough et al. 1996; Anderson et al. 1998; Turck-Chieze et al. 1998). Our absolute inversion for the sound-speed gradient suggests that the temperature gradient below the convective zone is closer to the adiabatic value than in the standard model, which could be an effect of weak penetrative convection contributing to the energy transport. What we have in mind here is that some of the most energetic plumes penetrate relatively deep below the bottom of the

convective zone and contribute (negatively) to energy transport, requiring a slightly higher temperature gradient to carry the excess flux outwards by radiation (see, e.g., Roxburgh 1996). Such convective motions would also contribute to mixing and therefore counteract the diffusion of *He*. A similar mixing effect may be caused by circulation in the layers below the convective zone, where the angular velocity adjusts from the angular variation in the convective zone to the constant value in the interior.

The most obvious explanation of the constant angular velocity in the interior is the effect of a magnetic field, a weak field $>10^{-3}$ gauss being sufficient to maintain almost uniform rotation. But such a field must be separated from the field in the convective zone and kept inside the core. One way that this could be achieved is through the effect of penetrative convective plumes, the boundary being where the pressure of the convective plumes balances that of the (weak) magnetic field.

We note that $W(r)$ inferred from the observations shows a much more gentle increase below the convective boundary, closer to a straight line, until $r \simeq 0.66R$ where it seems to have another quite rapid variation in slope, which might indicate the bottom of the partially mixed domain. This is consistent with the above suggestion that this is also the region in which the angular velocity adjusts to the constant value in the interior. At the base of the convection zone, the solar sound-speed gradient reveals a more gentle change in its slope (this conclusion also follows from the comparison of the approximation residuals; see Figs 1b–d).

Fig. 6(d) shows the region around $r = 0.2R$. The accuracy and stability of the inversions degrade significantly at these depths. A prominent difference between the Sun and the model is clearly seen, however, which corresponds to 0.2 per cent difference in $c^2(r)$ at $r \simeq 0.2R$ (see Fig. 4). Smaller values of the solar sound speed at $r \simeq 0.2R$ compared with standard model are a persistent feature well known in helioseismic inversions for over a decade (for recent results see, e.g., Gough et al. 1996 and Kosovichev et al. 1998). Smaller values of $W(r)$ should be interpreted as smaller values of the Brunt–Väisälä frequency [a similar inconsistency in N^2 was also indicated by the second-order asymptotic term $\Phi(\tilde{w})$ in the results of earlier asymptotic inversions; Vorontsov 1989]. The interpretation is probably related to some sort of mixing in the energy-generating core. The new feature of our present inversion is that the variation at $r \simeq 0.2R$ appears to be rather sharp. The origin of such a behaviour remains to be understood, but might be related to the steep outward increase in ^{3}He in this region in standard solar models. As shown by Dilke & Gough (1972) and Christensen-Dalsgaard, Dilke & Gough (1974), this steep gradient could drive a global instability. The evolution of this instability is still not well understood, but one possibility is that it breaks down into mild turbulence, causing mixing which prevents the growth of the instability (Roxburgh 1976, 1984). Such local mixing would modify the composition gradient and hence the sound speed profile.

Below $r \simeq 0.15R$, the observational data available do not show any significant deviation from the model (see also Fig. 4). We should emphasize, however, that this conclusion can not be considered as evidence that standard assumptions of the evolutionary model are basically correct: the seismic constraints on the structure of the inner solar core remain very weak.

5 CONCLUSIONS

Compared with earlier asymptotic inversions, the non-linear inversion based on the Born approximation gives a significant gain in both accuracy and spatial resolution. The accuracy of the description appears to be adequate enough for inverting the observational data which are currently available. The convergence and stability of the iterative inversion is provided, to a large extent, by the implicit constraint of monotonic behaviour of $c(r)/r$ with depth. Additional regularization is provided by using spline approximations.

The results obtained with solar data are in general agreement with recent results of linearized inversions based on the exact adiabatic equations. It appears possible, however, to refine some conclusions.

Deep in the convection zone, the solar sound-speed profile deviates substantially from model predictions, indicating that the adiabatic exponent is significantly closer to 5/3 than that determined by the OPAL equation of state.

The discontinuity in the slope of the sound-speed gradient at the base of the solar convection zone appears to be smaller than in the model. Together with a secondary rapid variation at $r \simeq 0.66R$, this feature may indicate that the most energetic convective plumes penetrate some way into the stable layers mixing the layers below the convective zone and contribute to the energy transport.

The difference between the inverted sound speed and that in solar models at $r \simeq 0.2R$ appears as a significantly sharper, more localized feature compared with previous inversions, probably due to better spatial resolution. The gradient of the solar sound speed has a very rapid variation here, which could signify another sharp boundary. The location of this feature in the region where the ^{3}He profile has a steep gradient suggests that it could be due to some local mixing driven by local instabilities, but the detailed interpretation of this feature remains to be studied.

ACKNOWLEDGMENTS

We are grateful to the MDI and GOLF teams for supplying their data, and to ESA/NASA for granting us Guest Investigator status on these experiments. The contribution of the GONG project is gratefully acknowledged. This work was supported in part by the UK PPARC under grants GR/K 94133, GR/L 39094 and GR/K 09526.

REFERENCES

Anderson E. et al., 1998, in Provost J., Schmider F.-X., eds, Sounding Solar and Stellar Interiors. Kluwer, Dordrecht, p. 151

Baturin V. A., Vorontsov S. V., 1998, in Provost J., Schmider F.-X., eds, Sounding Solar and Stellar Interiors. Obs. Cote d'Azur, Nice, p. 67
Brodsky M. A., Vorontsov S. V., 1993, ApJ, 409, 455
Christensen-Dalsgaard J., Dilke F. W. W., Gough D. O., 1974, MNRAS, 169, 429
Christensen-Dalsgaard J. et al., 1996, Sci, 272, 1286
Däppen W., Gough D. O., 1984, in Gabriel M., Noels A., eds, Theoretical Problems in Stellar Stability and Oscillations. Liège: Obs. de Liège, p. 264
Dilke F. W. W., Gough D. O., 1972, Nat, 240, 262
Gough D. O., 1986, in Gough D. O., ed., Seismology of the Sun and the Distant Stars. Reidel, Dordrecht, p. 125
Gough D. O., Vorontsov S. V., 1995, MNRAS, 273, 573
Gough D. O. et al., 1996, Sci, 272, 1296
Hill F. et al., 1996, Sci, 272, 1292
Iglesias S. A., Rogers F. J., 1991, ApJ, 371, 408
Kosovichev A. G. et al., 1998, in Provost J., Schmider F.-X., eds, Sounding Solar and Stellar Interiors. Kluwer, Dordecht, p. 203
Lazarek M. et al., 1998, Solar Phys., 175, 227
Marchenkov K. I., Roxburgh I. W., Vorontsov S. V., 1998, in Provost J., Schmider F.-X., eds, Sounding Solar and Stellar Interiors. Obs. Cote d'Azur, Nice, p. 101
Rhodes E. J., Kosovichev A. G., Schou J., Scherrer P. H., Reiter J., 1998, Solar Phys., 175, 287
Roxburgh I. W., 1976, in Bumba V., Klezeck J., eds, Basic Mechanisms of Solar Activity. Reidel, Dordecht, p. 453
Roxburgh I. W., 1984, in Maeder A., Renzini A. J., eds, Observational Tests of the Stellar Evolution Theory. Reidel, Dordrecht, p. 519
Roxburgh I. W., 1996, in Antia H. M., Chitre S. M., eds, Windows on the Sun's Interior. Bull. Astron. Soc. India, 24, 89
Roxburgh I. W., Vorontsov S. V., 1994a, MNRAS, 268, 880
Roxburgh I. W., Vorontsov S. V., 1994b, MNRAS, 268, 143
Roxburgh I. W., Vorontsov S. V., 1994c, in Gough D. O., Roxburgh I. W., eds, Proc. 6th IRIS Workshop, Cambridge, p. 57
Roxburgh I. W., Vorontsov S. V., 1994d, MNRAS, 267, 297
Roxburgh I. W., Vorontsov S. V., 1996, MNRAS, 278, 940 (R&V96)
Turck-Chieze S. et al., 1998, Solar Phys., 175, 247
Vorontsov S. V., 1989, SvA Lett., 15, 21
Vorontsov S. V., 1991, SvA, 353, 400
Vorontsov S. V., Shibahashi H., 1991, PASJ, 43, 739
Vorontsov S. V., Zharkov V. N., 1989, Astrophys. Space Phys. Rev., 7, 1
Vorontsov S. V., Baturin V. A., Gough D. O., Däppen W., 1994, in Chabrier G., Schatzman E., eds, The Equation of State in Astrophysics. Cambridge University Press, Cambridge, p. 545

This paper has been typeset from a TEX/LATEX file prepared by the author.